



OPEN

An optimized method for high-quality RNA extraction from distinctive intrinsic laryngeal muscles in the rat model

Angela M. Kemfack¹, Ignacio Hernandez-Morato^{1✉}, Yalda Moayed^{1,2} & Michael J. Pitman¹

Challenges related to high-quality RNA extraction from post-mortem tissue have limited RNA-sequencing (RNA-seq) application in certain skeletal muscle groups, including the intrinsic laryngeal muscles (ILMs). The present study identified critical factors contributing to substandard RNA extraction from the ILMs and established a suitable method that permitted high-throughput analysis. Here, standard techniques for tissue processing were adapted, and an effective means to control confounding effects during specimen preparation was determined. The experimental procedure consistently provided sufficient intact total RNA ($N=68$) and RIN ranging between 7.0 and 8.6, which was unprecedented using standard RNA purification protocols. This study confirmed the reproducibility of the workflow through repeated trials at different postnatal time points and across the distinctive ILMs. High-throughput diagnostics from 90 RNA samples indicated no sequencing alignment scores below 70%, validating the extraction strategy. Significant differences between the standard and experimental conditions suggest circumvented challenges and broad applicability to other skeletal muscles. This investigation remains ongoing given the prospect of therapeutic insights to voice, swallowing, and airway disorders. The present methodology supports pioneering global transcriptome investigations in the larynx previously unfounded in literature.

Vocal fold (VF) motion is regulated by the intrinsic laryngeal muscles (ILMs) that facilitate glottic activities integral to daily life, including voicing, swallowing, and breathing¹. To perform these roles, the ILMs control VF movement via complex neuromuscular activation^{2,3}. Upon contraction, the posterior cricoarytenoid (PCA) abducts the VFs, opening the glottis for swallowing and airflow during active and passive breathing³. In contrast, the thyroarytenoid (TA) muscles within the adductor complex adduct the VFs, a requisite of normal phonation⁴. Each set of muscles is innervated by ipsilateral branches of the recurrent laryngeal nerve (RLN). Following nerve injury, newly-formed axons from the proximal stump, directed in part by guidance cues, grow back to the denervated ILMs in an aberrant fashion. This non-selective reinnervation can result in synkinesis and VF paralysis with significant patient morbidity⁴⁻⁹. Effective treatment of nerve paralysis to re-establish normal VF function will require the restoration of the pre-injury innervation pattern. Further, therapeutic manipulation of the guidance cues expressed by the ILMs remains essential for rehabilitation. Evaluating gene expression in these muscles before and after RLN injury will provide the insight necessary to identify high-value targets for further research and therapeutic intervention. To this end, comprehensive RNA-Sequencing (RNA-Seq) of the distinctive ILMs will permit an unbiased, large-scale transcriptome assessment to identify unknown factors governing VF movement.

Minimal RNA degradation is paramount to reliable downstream analysis in any gene-profiling study, especially in robust sequencing techniques¹⁰. Whole-transcriptome RNA-Seq provides a broader, more precise characterization and distribution of mRNA transcripts compared to low-throughput methods (e.g., RT-qPCR, microarrays); thus, its technology warrants highly undegraded RNA samples¹¹. Until recently, insufficient RNA recovery hindered transcriptome investigations in skeletal muscles, given their characteristically high metabolic activity¹². In addition, the challenges of RNA extraction from post-mortem skeletal muscles are also significant across species. For instance, human post-mortem skeletal muscle analysis previously provided substandard RNA quality, summarized as RNA integrity numbers (RIN) ranging between 1.6 and 7.6¹³. This compromised RNA

¹Department of Otolaryngology-Head & Neck Surgery, Columbia University College of Physicians and Surgeons, New York, NY 10032, USA. ²Department of Neurology, Irving Medical Center, Columbia University College of Physicians and Surgeons, New York, NY, USA. ✉email: ih2302@cumc.columbia.edu

integrity restricted the downstream assessment to a low-throughput application and perturbed the RT-qPCR performance. In contrast, living tissue samples following human muscle biopsy yielded between 456 to 676 ng total RNA and 7.9 ± 0.6 RIN¹². Unfortunately, compared to other soft tissue types, the distinctive ILMs have not been amenable to RNA-Seq due to differences in cell characteristics¹⁴. Efforts to recover sufficient RNA from the distinctive ILMs have only been documented in low-throughput profiling techniques and histological studies due to their lower requisites for RNA quality^{15–22}. In this regard, fundamental knowledge gaps apropos the ILM innervation patterns reflect the unresolved challenges of high-quality nucleic acid input for bulk RNA-Seq. While efforts to sequence RNA from the skeletal muscles have emerged in recent literature, the methods described are unadoptable to this study, as they do not address the challenges of extracting high-quality RNA from the distinctive ILMs. In the rat, there is increasing evidence of bulk RNA-Seq using skeletal muscle in the hindlimb muscles^{8,23,24}. However, given their greater abundance of intrinsic RNA compared to the small ILMs, the proposed extraction strategies are insufficient for the ILMs as they do not account for the limited RNA content. A Parkinson's study performed by Lechner et al. (2021) assessed the RNA-Seq expression analysis from the rat TA. Although, their sequencing strategy enabled the input of low-throughput RNA extracts²⁵. This method, commonly known as TruSeq, requires a small sample size and has unique RNA specifications unamenable to other bulk RNA-Seq technologies²⁶. Other studies demonstrated successfully high-throughput RNA analysis from tissues excised from the human and rabbit larynxes^{27–29}. Unfortunately, they sampled all the soft tissue associated with the VFs, including VF mucosa and respiratory epithelium, rather than isolated ILM alone. Further, RNA extraction procedures described in a recent whole-genome profiling study from the bat cricothyroid muscles yielded variable and substandard RNA in the distinctive ILMs³⁰. Despite these studies, there remains a lack of publicly available data describing a functional and reliable extraction method from the distinctive ILMs for general RNA-Seq use.

The present study aimed to identify and resolve threats to consistent, high-quality RNA recovery in rat ILMs. Previous whole-genome analyses in the rat ILMs and other skeletal muscles utilized spin-column technology or reagents to separate the nucleic acids. Hence, similar protocols were evaluated in this investigation^{12,23–25,30}. Other methodological strategies for RNA purification, such as nucleic acid extraction via magnetic beads, were not applied here due to a lack of evidence of its use in rat skeletal muscles. Our evaluation of the diverse commercial protocols indicated that relevant challenges of high-quality RNA extraction from rat ILMs are likely due to the muscles' small size, unique cellular content, and fiber composition³¹. Other critical variables also influenced the quality of the RNA, namely, the condition of the tissue or the impact of degradation during processing steps. The vulnerability of RNA in rat ILMs is in contrast to findings that characterize skeletal muscle mRNA as highly stable relative to the liver, brain, and adipose tissue^{12–14}. This suggested that variable RNA stability across species, tissue types, and organ layers may require modified extraction strategies according to the specimen and sample size. To that extent, this study established a systematic, high-quality RNA extraction method from isolated post-natal rat ILMs that permitted RNA-Seq. By developing a suitable technique to minimize native and non-native derived degradation, enhanced RNA recovery was maintained. Identifying an ideal weight model also limited the impact of total tissue weight during handling steps. These findings demonstrate the critical factors of RNA isolation techniques that permit high-quality transcriptome analysis.

Results

Comparison of RNA extraction protocols. Standard extraction protocols were evaluated for the consistent production of high-quality RNA from isolated PCA, lateral thyroarytenoid (LTA), and medial thyroarytenoid (MTA) intrinsic laryngeal muscles. This study quantified the impact of mitigation strategies to establish optimal tissue processing conditions (a comprehensive workflow of the experimental design is summarized in Fig. 1). UV spectrophotometry (Nanodrop) was used to quantify RNA purity (A_{260}/A_{280} ratio), concentration (ng/ μ L), and total RNA yield (ng); while electropherogram (bioanalyzer) analysis provided RIN values for quality control (QC) assessment. RNA extraction using the following kits was performed according to the manufacturer's instructions unless otherwise stated. In compliance with RNA-seq recommendations, this study aimed to generate extracts with greater than 500 ng Total RNA, 1.98 A_{260}/A_{280} ratio, and 7.5 RIN. Qualifications for bioanalyzer assessment included sufficient total RNA recovery (> 200 ng), high purity (≥ 1.90), and no chemical contamination detection (Table 1).

Quick-RNA MicroPrep. The Quick-RNA MicroPrep protocol (Zymo Research) provided a cost-effective means for performing RNA isolations (Table 2). This column kit can be favorable for RNA extraction because it allows for polynucleotide isolation void of phenol contamination. Here, tissue samples were thawed and subsequently manually disrupted using RNase-free homogenization tubes. In preliminary evaluations of this protocol, favorable purities were observed (2.05 ± 0.09) (mean \pm SD) using only one tissue sample ($pt = 1$, where pt denotes pooled tissue); however, the amount of recovered RNA was low (247.76 ± 107.72 ng) and often did not meet the 200 ng requirement for RNA-Seq application (Table 1). To mitigate the low RNA yield, ILMs were pooled ($pt = 2$), prompting both an increase in total RNA output (791.69 ± 294.06 ng, $P > 0.99$) and a depreciation in the overall A_{260}/A_{280} ratio (1.63 ± 0.61 , $P = 0.99$) that were not statistically significant. Additionally, substantial variations in the quality of samples across assays discouraged the continued use of this protocol (Table 1).

RNeasy micro kit. The RNeasy Micro Kit (Qiagen) was performed under identical conditions for tissue processing as previously stated (Table 2). The advantages of the protocol included the absence of phenol detection in the recovered RNA and the short total procedure time. Using individual, frozen ILMs as starting material ($pt = 1$) resulted in a high variance in the A_{260}/A_{280} ratio (3.60 ± 2.92) and amount of recovered RNA (94.07 ± 68.61 ng) such that extracts performed in the same batch were inconsistent and rarely qualified for further processing

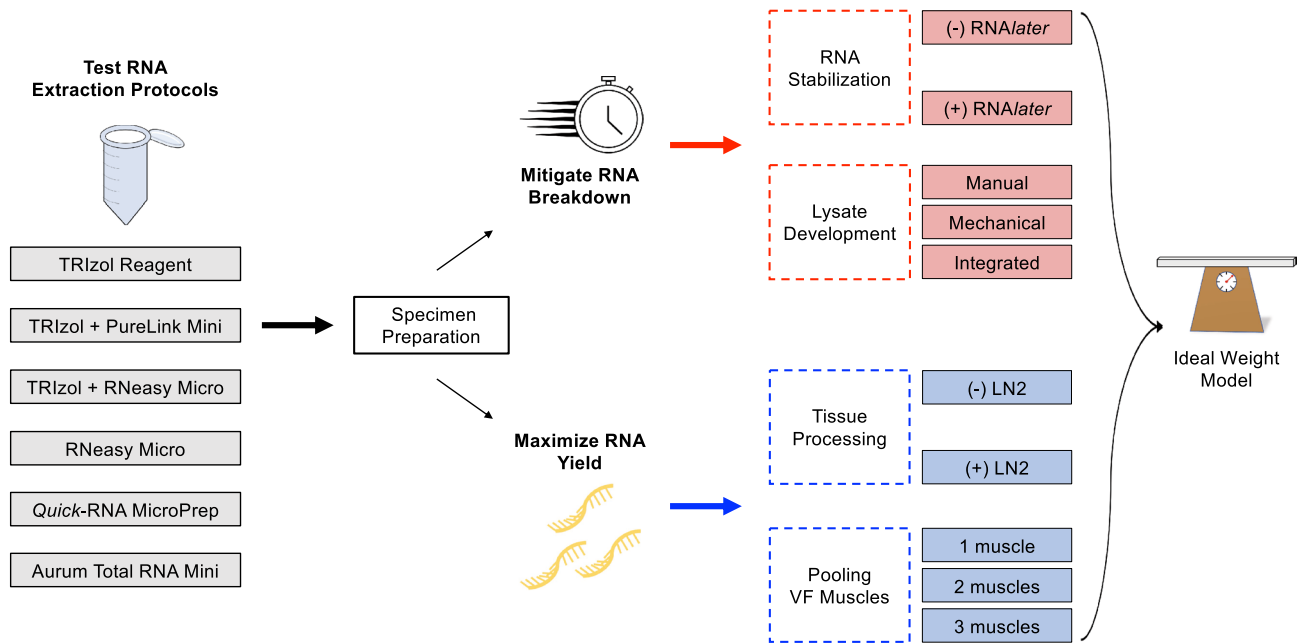


Figure 1. A schematic diagram of the experimental steps for high-quality RNA extraction from the vocal fold muscles.

(Table 1). Though increased tissue pooling ($pt=2$) resulted in a statistically significant difference in the overall A_{260}/A_{280} ratio ($P<0.0001$), the increase in total RNA yield ($P>0.99$) was nonsignificant (Table 1). This kit was discarded due to the discrepant RNA quantity and purity across assays (Table 1).

TRizol reagent. Trizol reagent (Invitrogen) yielded significantly higher total RNA quantities using individual ILMs compared to the results achieved using the spin-column kits (2458.84 ± 2070.48 ng, Quick-RNA, $P=0.05$; RNeasy, $P=0.004$) (Table 2). Limitations of this protocol included low A_{260}/A_{280} ratios (1.54 ± 0.10) in the recovered extracts, a 96.8% incidence (61 out of 63 samples) of phenol contamination across assays, and substantially longer procedure time than column-based methods; however, this procedure regularly provided RNA yields that exceeded the RNA-Seq sample requirements (Table 1). The cell lysis method was modified to mitigate the technical challenges. Optimal physical disruption parameters required rest periods flanking the manual lysing periods. To limit contamination, chloroform was reduced by 10–20 μ L per 1 mL of Trizol in 16 out of 63 samples. This study hypothesized that this reduction would account for the loss of guanidinium thiocyanate solution (TRizol) during rotor–stator disruption procedures. Here, differences in the overall purity ($P>0.99$) remained nonsignificant; however, this method provided the only uncontaminated samples in this trial. In addition, a slight reduction in the ratio of chloroform and prolonged incubation in isopropanol (~20 min) resulted in an individual RNA extract (1 out of 16 samples) with spectrophotometer measurements suitable for further processing ($A_{260}/A_{280}=1.92$; Total RNA = 7836.89 ng; phenol contamination = 0). Bioanalyzer assessment indicated a 7.0 RIN; however, these changes failed to provide comparable results beyond this sample.

½ TRizol reagent. Due to the promising results from reducing the amount of chloroform, this study examined the effect of further minimization of reagents. Hence, the volume ratio was altered to reduce the level of tissue exposure to the phenol-containing chloroform. Scaling down to 0.5X volumes of the reagents failed to reduce the incidence of contamination (100% phenol detection) and significantly increase the overall purity ($P>0.99$) relative to the former method (Table 1). As a result, this study terminated the continued implementation of this procedure.

TRizol reagent + RNeasy micro kit. Following the Furtado method³², the present study integrated the guanidinium thiocyanate solution (TRizol) and spin-column RNA purification (RNeasy) protocols to assess the moderation of purity and contamination. This technique did not reduce the detection of impurities (100% phenol contamination) or significantly increase the A_{260}/A_{280} ratios ($P>0.99$) and thus further trials were discontinued (Table 1).

TRizol reagent + PureLink RNA mini kit. The combination of the guanidinium thiocyanate solution (TRizol) and PureLink RNA Mini Kit (Invitrogen) protocols resulted in enhanced RNA quality (Table 2). Phase separation tubes were utilized to sequester the aqueous phase, reducing the incidence of phenol contamination by 47.3% compared to the guanidinium thiocyanate solution alone (26 out of 51 samples)³³. However, this modified protocol elicited a statistically significant decrease in RNA yield compared to the standard protocol ($pt=1$, $P<0.0001$, Table 1). The moderations applied here also increased the overall A_{260}/A_{280} ratios to 1.67 ± 0.13

Kits		Purification of RNA			Selection for Bioanalyzer			
		Samples (<i>n</i>)	Total RNA (ng)	260/280 ratio	Samples for RIN	Positive RIN	N/A RIN	RIN value
Quick-RNA microPrep	(<i>pt</i> = 1)	6	247.76 ± 107.72 (<i>p</i> = 0.94)	2.05 ± 0.09 (<i>p</i> > 0.99)	0	–	–	–
	(<i>pt</i> = 2)	9	791.69 ± 294.06 (<i>p</i> > 0.99)	1.63 ± 0.61 (<i>p</i> = 0.12)	0	–	–	–
	Total	15	574.11 ± 360.05 (<i>p</i> = 0.99)	1.80 ± 0.51 (<i>p</i> = 0.32)	0	–	–	–
RNeasy micro	(<i>pt</i> = 1)	6	94.07 ± 68.61 (<i>p</i> = 0.79)	3.60 ± 2.91 **** (<i>p</i> < 0.0001)	0	–	–	–
	(<i>pt</i> = 2)	24	700.09 ± 529.43 (<i>p</i> > 0.99)	2.12 ± 0.16 (<i>p</i> = 0.99)	0	–	–	–
	Total	30	578.89 ± 532.83 (<i>p</i> = 0.90)	2.42 ± 1.36 (<i>p</i> = 0.24)	0	–	–	–
TRIzol reagent	(<i>pt</i> = 1)	45	2458.84 ± 2070.48 **** (<i>p</i> < 0.0001)	1.52 ± 0.10 **** (<i>p</i> < 0.0001)	0	–	–	–
	(<i>pt</i> = 2)	18	4148.15 ± 1996.87 **** (<i>p</i> = 0.0001)	1.57 ± 0.09 ** (<i>p</i> = 0.002)	0	–	–	–
	Total	63	2941.50 ± 2174.27 **** (<i>p</i> < 0.0001)	1.54 ± 0.1 **** (<i>p</i> < 0.0001)	2	1/2	1/2	7.0 ± 0.0
½ TRIzol reagent	(<i>pt</i> = 1)	12	4430.11 ± 4049.31 **** (<i>p</i> = 0.0001)	1.51 ± 0.11 ** (<i>p</i> = 0.004)	0	–	–	–
TRIzol and RNeasy micro	(<i>pt</i> = 1)	3	1309.35 ± 355.11 (<i>p</i> > 0.99)	1.54 ± 0.04 (<i>p</i> = 0.59)	0	–	–	–
TRIzol and PureLink RNA mini	(<i>pt</i> = 1)	51	688.65 ± 611.70 (<i>p</i> = 0.97)	1.67 ± 0.13 **** (<i>p</i> < 0.0001)	19	12/19	7/19	4.2 ± 1.3 **** (<i>p</i> < 0.0001)
Aurum	(<i>pt</i> = 1)	15	284.96 ± 165.61 (<i>p</i> = 0.58)	2.42 ± 0.35 (<i>p</i> = 0.63)	0	–	–	–
	(<i>pt</i> = 2)	27	311.47 ± 260.37 (<i>p</i> = 0.29)	2.25 ± 0.62 (<i>p</i> > 0.99)	0	–	–	–
	Total	42	302.01 ± 229.18 (<i>p</i> = 0.11)	2.31 ± 0.54 (<i>p</i> = 0.78)	15	15/15	–	5.2 ± 1.4 **** (<i>p</i> < 0.0001)
Aurum and RNAlater	(<i>pt</i> = 3)	48	658.80 ± 330.17 (<i>p</i> = 0.96)	2.27 ± 0.42 (<i>p</i> = 0.97)	25	25/25	–	8.0 ± 0.4 (<i>p</i> = 0.68)
Proposed method (Aurum)	(<i>pt</i> = 3)	68	981.28 ± 446.11	2.14 ± 0.09	68	68/68	–	7.8 ± 0.4

Table 1. Assessment of protocols for RNA extraction from the rat intrinsic laryngeal muscles (ILMs). An analysis of variance (one-way ANOVA followed by Tukey's post-hoc test) was used to compare the commercial protocols to the experimental method ($P < 0.0001$). The *pt* indicates the number of pooled tissues per extract, while *n* represents the number of replicates. The RNA concentration (ng/μl) (shown as ng total RNA) and 260/280 ratio were measured using a Nanodrop Spectrophotometer. Data are presented as mean ± SD; $P < 0.05$. RNA degradation was assessed using Agilent 2100 Bioanalyzer. The selection for Bioanalyzer indicates the number of samples applicable for RIN (RNA integrity number) analysis. Individual sample qualifications for QC were selected based on the starting material requirements for RNA-Seq (i.e., greater than 200 ng total RNA and 1.90 purity) and the presence of impurities in the extract. N/A RIN denotes samples RIN values that were not calculable.

($P = 0.99$) though this change was not statistically significant. This method provided several samples with spectrophotometer measurements that warranted bioanalyzer assessment despite the lower total RNA yield (Table 1). Electropherogram analysis detected only one extract with a RIN > 7.0 (7.2 RIN), while most extracts contained relatively degraded RNA with RIN values ranging from 2.6 to 5.4. In addition, the quantity of non-calculable RIN values discouraged ongoing manipulation of this technique (Table 1). Consequently, the guanidinium thiocyanate solution was discarded because this study was unable to establish conditions to isolate RNA with acceptable purities using the reagent.

Aurum total RNA mini kit. The Aurum kit (Bio-Rad) provided the most favorable A_{260}/A_{280} ratios (2.31 ± 0.54) throughout this investigation (Tables 1 and 2). Despite the nonsignificant differences in purity compared to other tested column-based methods (1.80 ± 0.51 for Quick-RNA MicroPrep, $P = 0.72$ vs. Aurum kit; 2.42 ± 1.36 for RNeasy Micro, $P = 0.62$ vs. Aurum kit) the resultant A_{260}/A_{280} ratios using this spin-column (Aurum) kit did not extend below 1.96. Though most extracts were inapplicable for meaningful RNA-seq analysis, this kit

	QuickRNA microprep	RNeasy micro	TRIzol reagent	TRIzol + RNeasy micro	TRIzol + PureLink RNA mini	Aurum total RNA mini
Starting material	≤ 10 mg tissue (stored at -80°C)	< 5 mg tissue (stored at -80°C)	50–100 mg tissue (stored at -80°C)	< 15 mg tissue (stored at -80 °C)	≤ 200 mg tissue (stored at -80 °C)	≤ 40 mg thawed tissue (stored at -80°C)
Approx. preparation time	~20–30 min	~30–40 min	~1–2 h	~1–2 h	~60 min	~30–60 min
Binding capacity	10 µg total RNA	100 µg total RNA	N/A	100 µg total RNA	1000 µg total RNA	> 100 µg total RNA
Storage	RT	RT	15–30 °C	15–30 °C/RT	15–30 °C/RT	RT
DNase digestion	Yes	Yes	No	No	No	Yes
Elution volume	20 µl	10–14 µl	N/A	20 µl	30 µl	30 µl-2 × 40 µl
Advantages	Rapid procedure	Rapid procedure	High RNA yield	High RNA yield	Reduced contamination	Purity > 1.96
Disadvantages	Inconsistent recovery	Inconsistent recovery	Low purity	Low purity	Low purity	Purity > 2.2
	Low RNA yield	Low RNA yield	Phenol contamination	Phenol contamination	Phenol contamination	Low RNA yield

Table 2. An overview of the specifications of the evaluated commercial kits and protocols.

provided no invalid RIN values ($RIN = 5.19 \pm 1.39$, Table 1). These results indicated significantly increased RIN compared to the combined guanidinium thiocyanate (TRIzol + PureLink) method ($P < 0.0001$, Table 1). However, a shortcoming of this column kit was its feasibility of recovering at least 500 ng of total RNA from a single ILM ($pt = 1$) or two pooled ILMs ($pt = 2$, Table 1). This protocol was selected for further optimization due to its more manageable complications comparatively. The present study hypothesized that modified specimen conditions and starting material ($pt = 3$) would improve RNA integrity yield, respectively. While the applied changes significantly increased the RIN ($P > 0.0001$), these changes were insufficient to promote protocol systemization or consistent recovery (Table 1).

Impact of RNA stabilizing mechanisms. Stabilization of endogenous RNA by ribonuclease (RNase) inhibiting reagents improved RNA integrity compared to the standard method (Fig. 2a). The applied RNase-inhibiting reagent (RNAlater), which hinders RNase activity through precipitation and metal chelation¹⁰, significantly increased the RIN in the overall model ($P < 0.0001$, Fig. 2a, Table 1). RNA isolated under standard conditions resulted in considerable RNA degradation shown by the migration of noisy 28S/18S ribosomal peaks (Fig. 2b–d, left). Electropherogram peaks showed general depreciation of RNA molecules and insufficient total RNA recovery using standard tissue handling procedures (Fig. 2b–d, left). Alternatively, the addition of RNase-inhibiting reagents caused more distinct ribosomal RNA peaks and increased the RIN (Fig. 2b–d, right). Low 28S/18S ratios (below 2.0) also revealed the vulnerability of RNA during isolation steps; however, the reliability of the 28S/18S ratios as an indication of relative degradation is unclear (Fig. 2b,d). Together, the low 28S/18S ratios and the small, rounded peaks at the baseline observed in the electrophoretic traces indicated that RNase-inhibiting reagent treatment provided partial stabilization (Fig. 2b–d, right). Beyond its indispensable inhibitory properties, overnight incubation in RNase-inhibiting reagent also promoted the hardening of the muscle fibers, which increased the labor required to affect cell lysis.

Homogenization parameters for high-quality RNA. Developing an effective cell lysis method for adult rat ILMs required a systematic assessment of manual and mechanical homogenization strategies. Manual techniques involved physical breakdown via disposable pestle in specialized RNase-free homogenization tubes. Mechanical rotor–stator homogenization (TissueRuptor II) provided high-speed, automated tissue breakdown through replaceable probes. Finally, an integrated lysis method that incorporated both strategies was also adopted.

Evaluation of different homogenization methods suggested RNA yield and RIN were dependent on the cell lysis method, while purity was not ($P = 0.33$). Across global experiments ($pt = 3$), the integrated homogenization method increased the recovery of RNA (887.59 ± 216.18 ng) and demonstrated significant differences compared to the manual (423.77 ± 143.98 ng, $P = 0.001$) and mechanical methods (372.15 ± 145.10 ng, $P = 0.0004$) (Fig. 3a). Physical homogenization provided nonsignificant but comparatively higher RIN (8.4 ± 0.1) than the combined (8.1 ± 0.1 , $P = 0.93$) and the rotor–stator lysis methods (7.4 ± 0.6 , $P = 0.06$) in the overall model ($P = 0.59$, Fig. 3b). Though not significant, the depreciation of RNA recovery and RIN at high rotor–stator speeds implicated the role of mechanical lysis in RNA degradation. The range of RNA quantity using this disruption technique (3.49–1535.24 ng) also supported findings that identify aggressive rotor–stator use as a source of RNA damage³⁴. Ultimately, the integrated lysis strategy at medium rotor–stator speeds provided the most favorable RNA extracts due to its propensity to promote considerable RNA recovery with less damage. This study advises manual homogenization if labor and limited RNA quantity are not of a concern. Collectively, these findings demonstrated a critical dichotomy in the breakdown of ILMs, that is, resilient fibers and limited, fragile RNA.

Establishing the ideal weight model. The evaluation of total RNA recovery attributable to the span of rotor–stator use (Supp. Fig. S2) suggested a critical range of breakdown that provides maximal RNA recovery. In our experimental trials, the assessment of optimal rotor–stator durations indicated variable periods of lysis between the ILMs, their anatomical location (i.e., right and left side), and the respective assay. The present study surmised that these discrepancies reflected the weight of starting material, a confounding variable in the cel-

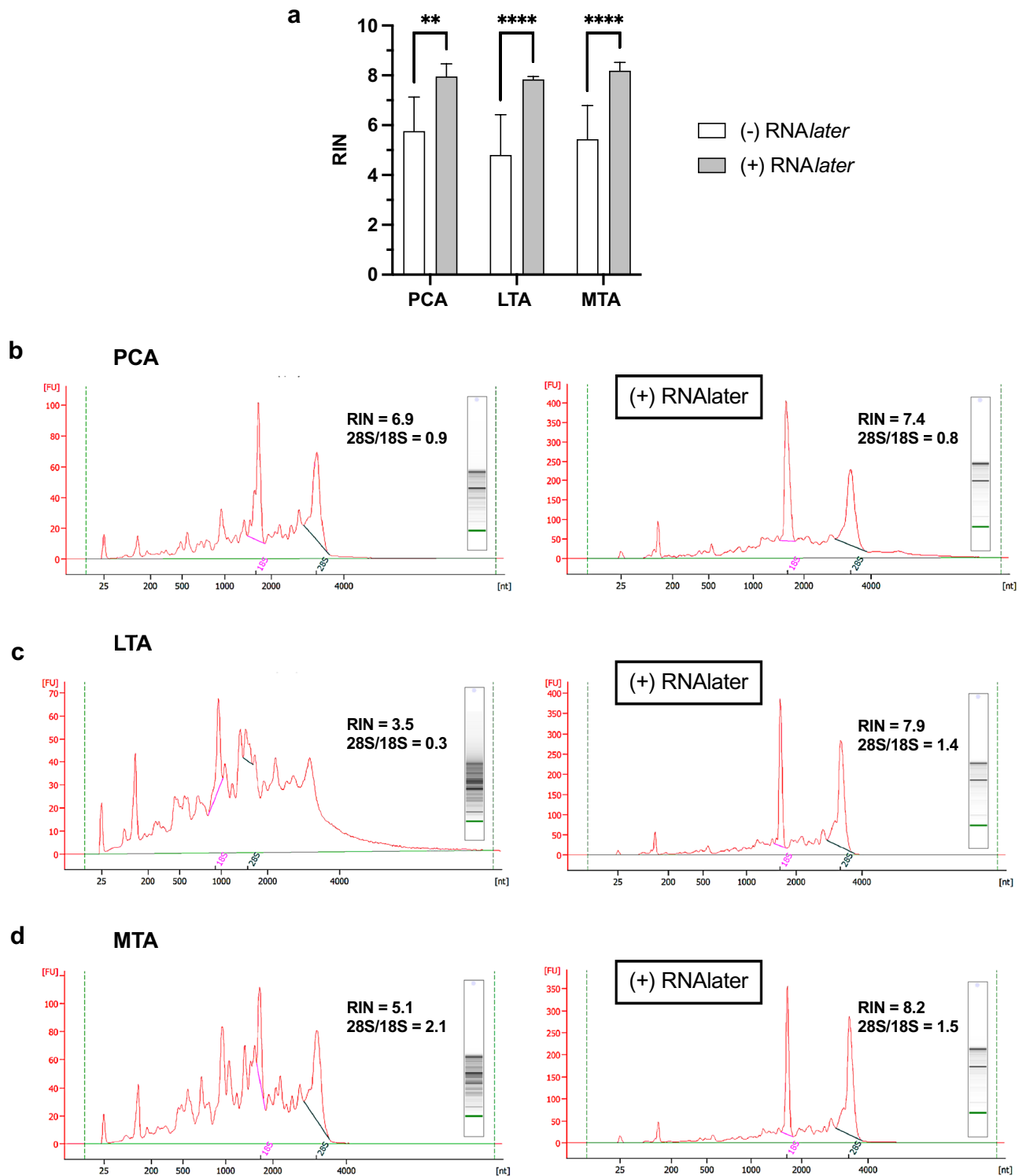


Figure 2. Comparison of RNA stability under standard conditions and following experimental application of RNase-inhibiting reagent (RNAlater). **(a)** Significant differences were found in RIN between the experimental (+ RNAlater) (PCA, $N=7$; LTA, $N=5$; MTA, $N=9$) and standard (-RNAlater) methods (PCA, $N=5$; LTA, $N=6$; MTA, $N=6$). **(b–d)** Electropherograms from the standard (*left*) are juxtaposed with the experimental method (*right*). Electropherograms provided by Agilent 2100 Bioanalyzer Pico Chip were visualized using 5 μ L total RNA. Electrophoretic traces, RIN, 28S/18S ratios, and gel electropherograms that were representative of the global results are displayed for the PCA **(b)**, LTA **(c)**, and MTA muscles **(d)**. 28S ribosomal peaks are shown in magenta, and 18S ribosomal peaks are shown in green. Analysis of variance was performed using a two-way ANOVA with Posthoc tests. The data is expressed as mean \pm SD. * means $P < 0.05$; ** $P < 0.01$; *** $P < 0.001$; **** $P < 0.0001$. Original gels are presented in Supplementary Fig. S1.

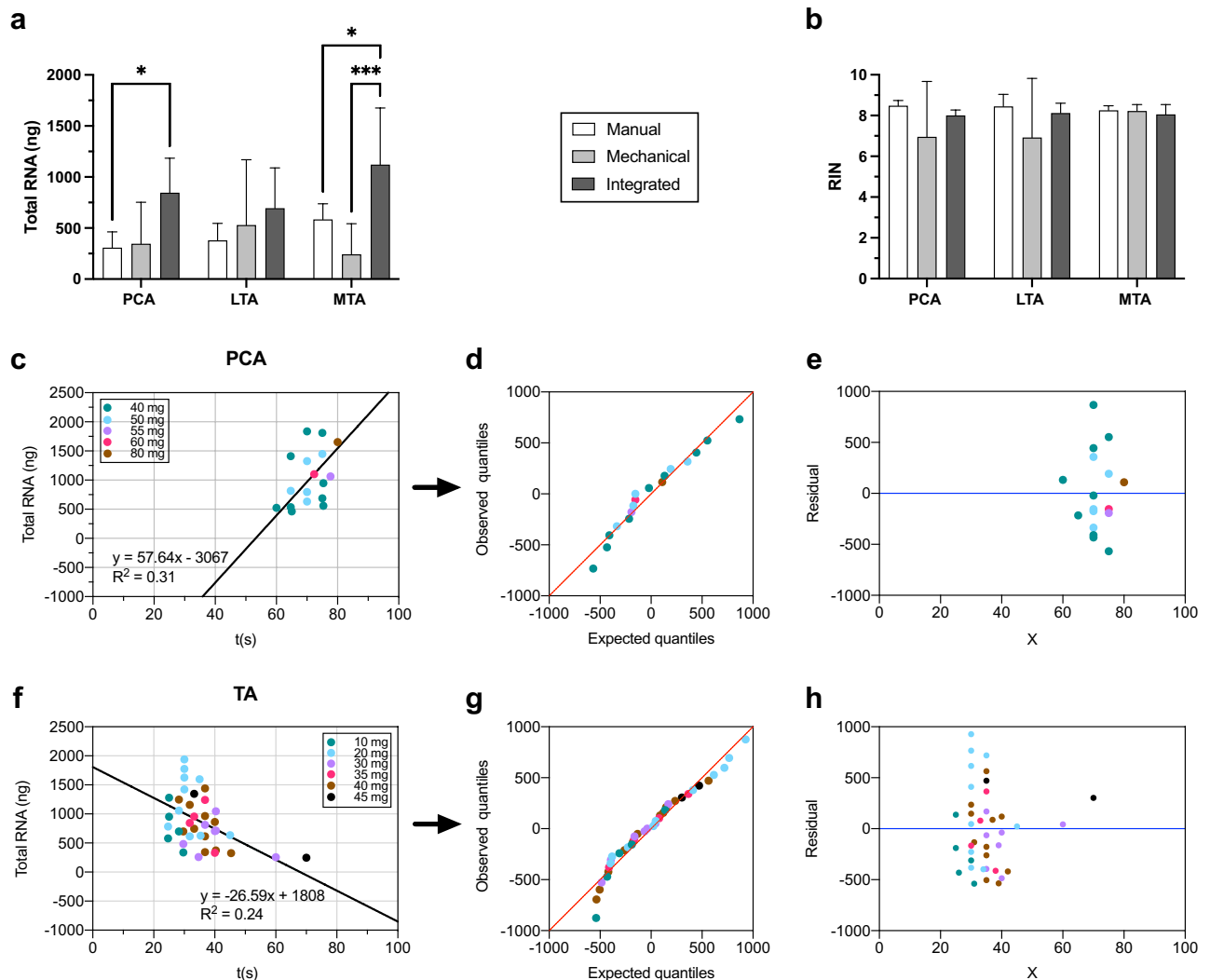


Figure 3. The impact of the novel disruption paradigm on RNA recovery. Total RNA (ng) was determined by computing the volume of the RNA elution buffer (38 μ L) and the RNA concentration (ng/ μ L) measured via a Nanodrop Spectrophotometer at 260 nm. **(a)** Comparison of the total RNA extraction (per respective ILM) between the integrated method (experimental) (PCA, $N=6$; LTA, $N=6$; MTA, $N=6$) relative to the manual and mechanical techniques (PCA, $N=6$; LTA, $N=6$; MTA, $N=6$). **(b)** RIN values were obtained using different homogenization methods. The Agilent 2100 Bioanalyzer Pico Chip assay indicated the RNA stability of extracts. **(c,f)** Linear regression analysis correlating disruption time, tissue weight, and total RNA recovery from **(c)** PCA ($m = 57.64$, $R^2 = 0.31$) and **(f)** TA muscles ($m = -26.59$, $R^2 = 0.24$). **(d,g)** Q-Q plot of the weight distribution in the PCA **(d)** and TA **(g)** muscles. **(e,h)** Residual analysis for validation of the linear regression in the PCA **(e)** and TA **(h)** muscles. Analysis of variance was performed using a two-way ANOVA with Posthoc tests. The data is expressed as mean \pm SD. * means $P < 0.05$; ** $P < 0.01$; *** $P < 0.001$; **** $P < 0.0001$.

lular disruption process. Furthermore, investigators observed up to ten-fold differences in RNA quantity from -10 to 10 s changes in the rotor–stator span. An ideal weight model was developed by measuring total tissue weights ($pt=3$) and evaluating the results from varying disruption times across several assays. These investigations allowed the present study to systematize the experimental procedure by identifying the upper and lower limits that ensured considerable intact RNA yields given the tissue characteristics. Table 3 presents a range of weights and disruption times that provided the greatest, undiminished recovery. Similar impacts to the RIN were observed in some but not all cases; hence, this study only presents the total RNA yield, which revealed a more undeviating pattern.

Linear regression was implemented to determine the correlation between the ILM type, pooled tissue weight, period of rotor–stator lysis, and RNA yield (Fig. 3c,f). This revealed opposing regressions between the PCA and TA muscles. More specifically, sufficient RNA recovery was only feasible at >1 min using the abductor muscle (Fig. 3c,f). Shorter rotor–stator durations did not provide lysates that could readily pass through the silica membrane. In contrast, the total RNA in the TA muscles was reduced by prolonged homogenization with optimal times ranging from 25 to 40 s. Diverging from the PCA muscle, raw data from the LTA and MTA muscles were compounded because it was observed that they required similar disruption times ($R^2 = 0.24$, Fig. 3d). Given the

Muscle type					
PCA		LTA		MTA	
Mass (mg) ^a	Time (s)	Mass (mg) ^a	Time (s)	Mass (mg) ^a	Time (s)
				10 mg (n = 5)	25–30 s
		20 mg (n = 2)	35 s	20 mg (n = 9)	30 s
		30 mg (n = 4)	35 s	30 mg (n = 4)	30–35 s
40 mg (n = 9)	65–70 s	40 mg (n = 11)	35–40 s	40 mg (n = 2)	30–35 s
50 mg (n = 6)	70–75 s				
60 mg (n = 3)	75 s				

Table 3. Recommended range of optimal disruption times using adult rat ILMs. The appropriate span of rotor–stator disruption attributed to the rodent stage, the total weight of the specimen, and muscle type are shown. The listed ranges were collated based on extraction efficiency. ^aTotal muscle weights using 3 pooled tissues.

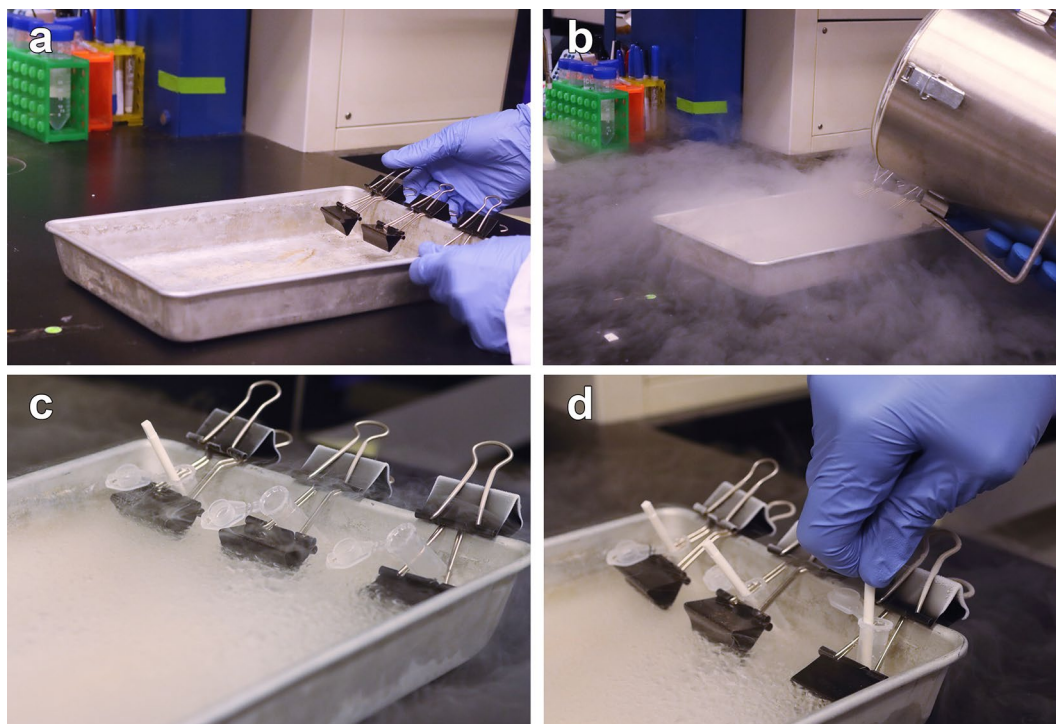


Figure 4. Setup of the apparatus that facilitated cryogenic disruption in RNase-free tubes as an alternative to tissue grinding via mortar and pestle. (a) Medium binder clips were attached to the lip of a surgical tray. Both metal wire arms of a complementary binder clip were wedged securely between the gripped section and the interior lip. (b) Liquid nitrogen (approx. 1 L) was poured directly into the tray. (c) BioMasherIII tubes containing the muscle fibers were stabilized by the looped arms of the attached clip. Once snap-frozen, tissues were crushed using disposable pestles. (d) Tissue grinding in liquid nitrogen ensued until fibers were finely broken down.

larger size of the PCA muscles, their homogenization needed to be longer to break down the tissue and provide sufficient nucleic acid yields ($R^2 = 0.31$, Fig. 3c). Visualization of the observed and theoretical quantiles indicated a normal distribution of the presented data (Fig. 3d,g). The residual plots confirmed the accuracy of the linear regression (Fig. 3e,h). The results suggest variation in RNA recovery was attributable to the tissue density, weight, and disruption span (Fig. 3c–g).

Effects of cryogenic grinding on RNA quality. A simple instrument, which circumvented cross-contamination and thawing, was developed to facilitate the breakdown of tissue hardened by RNase-inhibiting reagent (Fig. 4). Initial tissue grinding in liquid nitrogen maximized the capacity of the silica membrane (40 ± 20 mg). In addition, it reduced the instance of column clogging and hole formation from insufficient homogenization. The adapted method for cryogenic disruption significantly improved the RNA recovery in the overall model (Fig. 5a). Generally, this modification raised RNA quantities to 1003.64 ± 161.181 ng relative to the

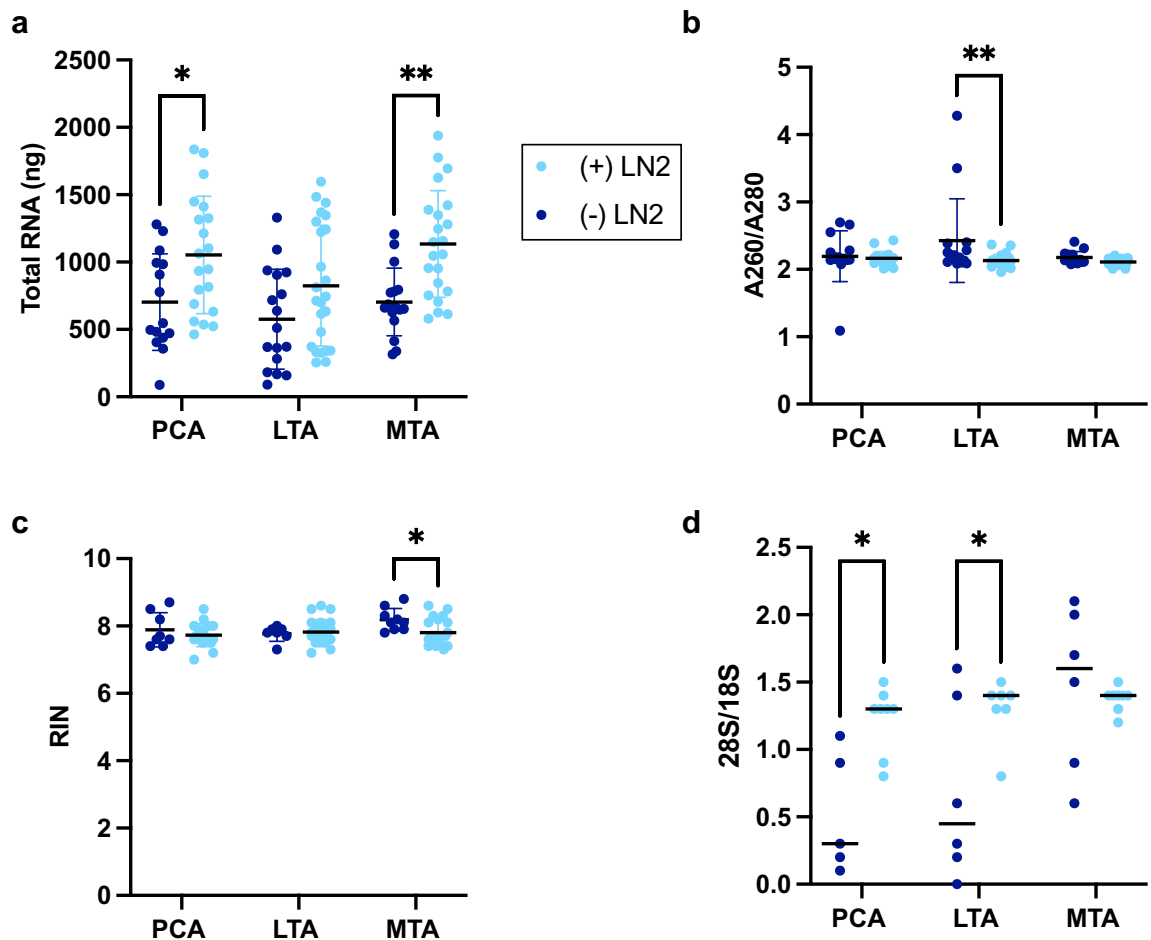


Figure 5. The influence of adapted cryogenic disruption on total RNA recovery under experimental (+LN2) and standard conditions (−LN2). Data points plotted in dark blue signify standard conditions, or samples processed without liquid nitrogen (PCA, $N=15$; LTA, $N=17$; MTA, $N=16$), while the light blue denotes experimental conditions, or the samples that were processed with liquid nitrogen (PCA, $N=24$; LTA, $N=24$; MTA, $N=22$). The vertical lines associated with the respective colors represent the error, while the horizontal lines (dark black) indicate the mean. **(a)** Comparison of total nucleic acid extraction, determined by Nanodrop Spectrophotometer at 260 nm, under the experimental and standard conditions. **(b)** Changes in A_{260}/A_{280} , measured via Nanodrop, under experimental and standard conditions. **(c)** The impact of the RIN, provided by the Agilent 2100 Bioanalyzer Pico chip, due to cryogenic disruption under experimental and standard conditions. **(d)** Analysis of the tendencies of the 28S/18S ratios under experimental and standard conditions. Analysis of variance was performed using a two-way ANOVA with Posthoc tests. The data is expressed as mean \pm SD. * means $P < 0.05$; ** $P < 0.01$; *** $P < 0.001$; **** $P < 0.0001$.

standard method (661.44 ± 73.31 ng, $P < 0.0001$). A significant increase in RNA yield was observed in the PCA ($P = 0.03$) and MTA ($P = 0.003$) muscles, while the changes observed in the LTA were not significant ($P = 0.15$, Fig. 5a). On the other hand, significant differences in RNA purity were revealed in the LTA compared to other ILMs ($P = 0.004$) and the overall model ($P = 0.01$, Fig. 5b). Despite observing slight reductions in the experimental RIN compared to standard conditions, two-way ANOVA analysis revealed no significant changes overall in RNA stability due to the applied method ($P = 0.06$, Fig. 5c). Significant differences attributable to cryogenic disruption were only demonstrated in the RIN from MTA muscles ($P = 0.02$, Fig. 5c). The MTA was the only muscle with no significant improvements to the 28S/18S ratios ($P > 0.99$, Fig. 5d). However, two-way ANOVA analysis indicated significantly increased 28S/18S ratios from cryogenic disruption across the overall muscle types ($P = 0.004$, Fig. 5d).

Validating the applied tissue pooling strategy. Various pooling strategies ($pt = 1-3$) were evaluated to determine the optimal number of muscles per sample to isolate sufficient quantities of RNA for sequencing (Fig. 6). In initial trials using the preferred *Aurum Total RNA Mini Kit*, pooling one or two ILMs resulted in inadequate total RNA yields (Table 1). However, the progressive increase in RNA recovery in the aforementioned experimental steps reconsidered the need for tissue pooling, as such different conditions were tested. Two-way ANOVA analysis indicated significant differences in the total RNA yield attributable to tissue pooling ($P < 0.0001$, Fig. 6a). These evaluations suggested that consistent high RNA recovery (> 200 ng) is not achiev-

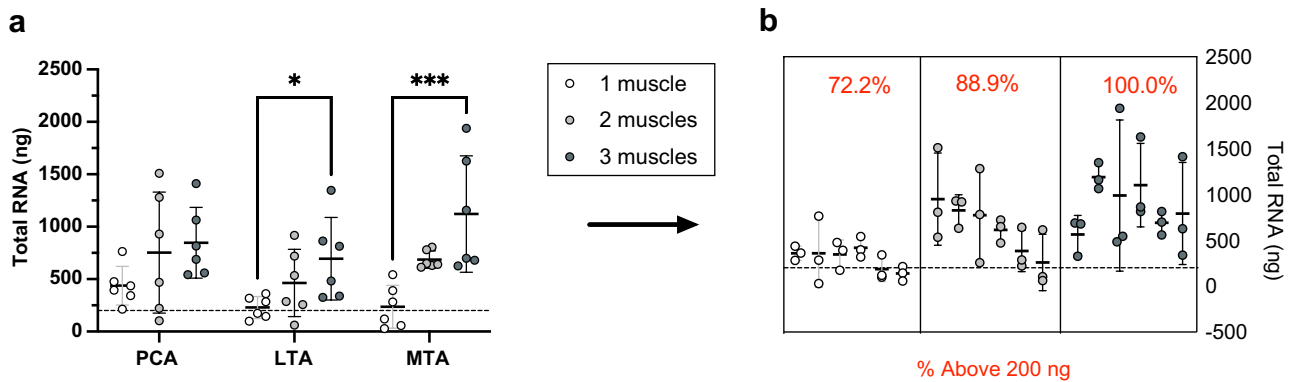


Figure 6. Validation of the pooling strategy. Total RNA was calculated from the volume of the RNA elution buffer (38 μL), and the RNA concentration (ng/ μL) was measured via a Nanodrop Spectrophotometer at 260 nm. The black dashed lines denote the target yield of RNA for the different pooling strategies evaluated (200 ng). (a) Comparison of total RNA recovery from 1 pooled muscle (PCA, $N=6$; LTA, $N=6$; MTA, $N=6$), 2 pooled muscles (PCA, $N=6$; LTA, $N=6$; MTA, $N=6$), and 3 pooled muscles (PCA, $N=6$; LTA, $N=6$; MTA, $N=6$). (b) Nested perspective showing the percentage of extracts greater than 200 ng (red). Analysis of variance was performed using a two-way ANOVA with Posthoc tests. The data is expressed as mean \pm SD. * means $P < 0.05$; ** $P < 0.01$; *** $P < 0.001$; **** $P < 0.0001$.

Muscle	N	260/230	260/280	Total RNA (ng)	RIN	28S/18S	No. reads	Pseudo aligned reads	Mapping ratio
PCA	29	1.03 \pm 0.53	2.15 \pm 0.09	1513.68 \pm 860.68	7.8 \pm 0.3	1.4 \pm 0.2	4.19E+07 \pm 7.23E+06	3.33E+07 \pm 5.88E+06	79.4 \pm 1.5
LTA	30	1.08 \pm 0.47	2.12 \pm 0.06	1436.82 \pm 903.31	7.9 \pm 0.4	1.4 \pm 0.2	4.22E+07 \pm 7.42E+06	3.31E+07 \pm 5.83E+06	78.5 \pm 1.8
MTA	29	1.10 \pm 0.45	2.13 \pm 0.06	1081.44 \pm 397.08	8.1 \pm 0.5	1.4 \pm 0.2	4.04E+07 \pm 6.82E+06	3.13E+07 \pm 5.45E+06	77.5 \pm 1.7
Control	2	0.85 \pm 0.36	2.14 \pm 0.19	413.55 \pm 25.63	8.1 \pm 0.7	1.6 \pm 0.1	4.17E+07 \pm 7.22E+06	3.37E+07 \pm 5.99E+06	80.9 \pm 0.3

Table 4. Summary of the downstream diagnostics from experimental total RNA extracts ($N=90$). RNA samples were sequenced using a standard RNA-Seq pipeline (Illumina NovaSeq 6000), and sequencing reads were quantified using Kallisto. Note, the controls in this experiment were (1) RNA extracts from the right ILMs aggregated and (2) RNA extracts from all paired ILMs combined.

able using individual ILMs. Pooling a few muscles, however, significantly enhanced RNA recovery ($pt=1$ vs 3, $P=0.0004$, Fig. 6a). Subsequent trials with two pooled ILMs ($pt=2$) resulted in sufficient RNA quantities in most (88.9%) but not all cases ($P=0.06$, Fig. 6b). In contrast, pooling ILMs from three adult rats (300 g) consistently produced the recommended concentrations for RNA-seq (100% of samples, $N=18$, Fig. 6b). Trials with three muscles demonstrated sufficient extraction across the PCA (846.54 \pm 336.87 ng), LTA (694.89 \pm 394.07 ng, $P=0.05$), and MTA muscle (1121.35 \pm 555.19 ng), which was not readily observed using fewer pooled muscles (Fig. 6). Moreover, the advantage of pooling three muscles over two is assurance the samples will qualify for downstream processing.

An overview of the experimental protocol. The collective experimental techniques provided ($N=68$) RIN values from 7.0 to 8.6 (7.8 \pm 0.4) with no RNA yields below 250 ng (981.28 \pm 446.11, Table 1). Ultimately, the applied experimental modifications in conjunction with the Aurum Total RNA Mini kit significantly improved RNA recovery compared to other evaluated protocols (Table 1). Functional RNA extraction from rat ILMs required RNase-inhibiting reagents during surgical steps and overnight incubation for nucleic acid stabilization. High-quality RNA extracts were achieved by implementing the integrated (manual and mechanical) cell lysis strategy, establishing the ideal weight model, and adapting cryogenic disruption. Finally, pooling three ILMs permitted consistent and sufficient total RNA yields. The reproducibility of the experimental method was confirmed using P15 and P32 (~115 g) rats, which validated the effectiveness of the experimental conditions (Supp. Fig. S3). Table 4 summarizes RNA-Seq (NovaSeq) data analysis taken from 90 RNA samples, with RIN ranging between 7.0 to 9.3. Only six samples were between 7.0 and 7.4. The remaining 84 samples (RIN = 8.0 \pm 0.4) ranged from 7.5 to 9.3. RNA-Seq diagnostics indicated that the few samples with lower RIN were still within the range according to the sequencing alignment score (Table 4). Principal component analysis and normalization factors also showed that 98% of the inter-intra-variability was maintained within the first two principal components, suggesting a reliable gene assessment (Fig. 7).

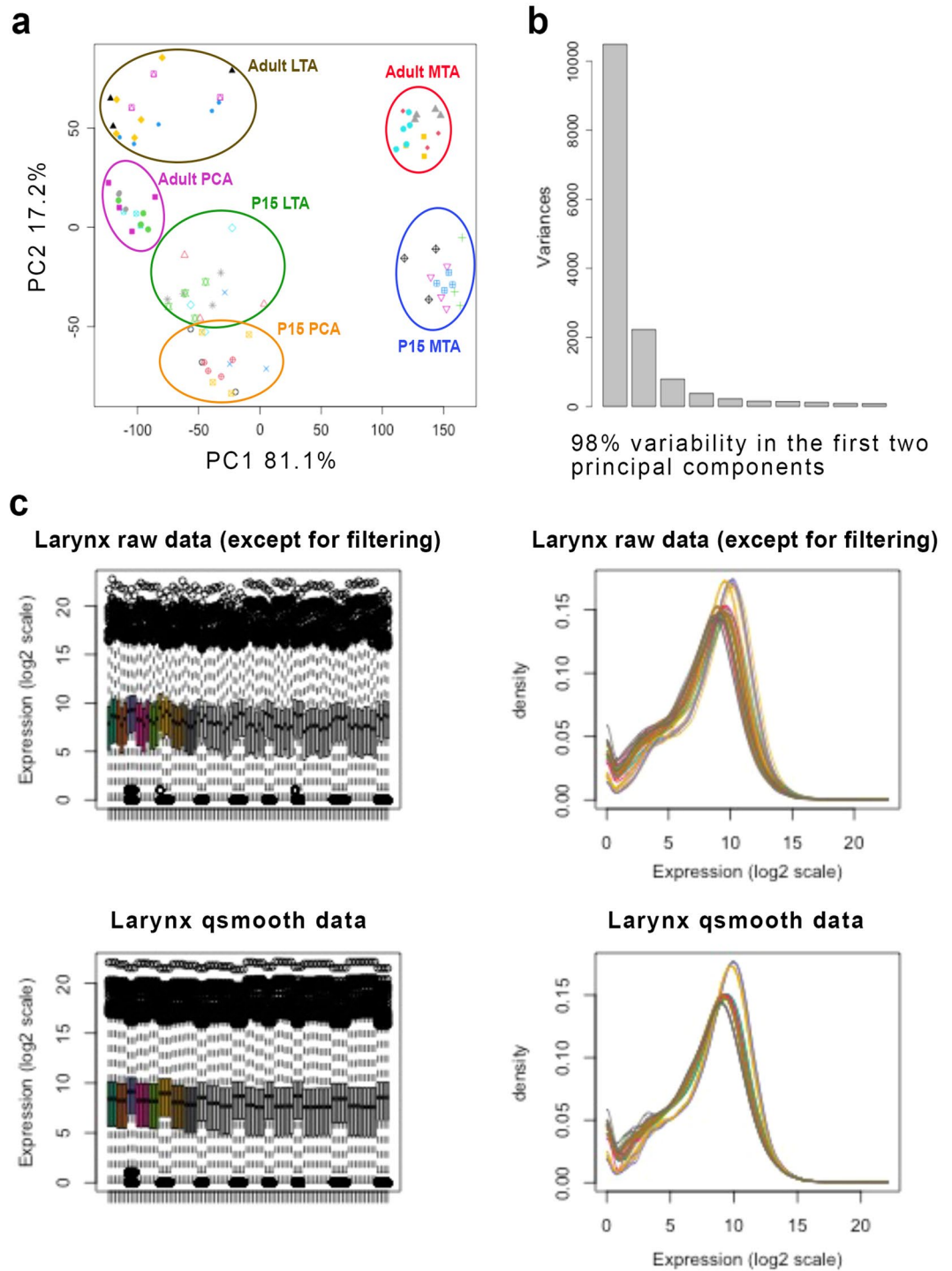


Figure 7. RNA-Seq diagnostics. The samples were sequenced using the NovaSeq 6000 platform (Illumina, Inc) (a) The principal component analysis shows a global summary based on the variance of the log₂ concentration. (b) The scree plot shows the relative amount of variance in each principal component. (c) Samples were normalized with qsmooth as shown in raw diagnostics data.

Discussion

The present study mitigated and quantified the factors that decreased total RNA recovery from rat vocal fold muscles. In identifying these significant contributors, this investigation established a systematic protocol that consistently produces high-quality RNA extracts. Our findings demonstrate that high-quality RNA extraction from isolated PCA, LTA, and MTA muscles is contingent on adapted tissue preparation steps. This research has pioneered a reproducible protocol that provides RNA extracts suitable for varied bulk RNA-Seq methods.

Comparisons of the purification procedures suggested that standard tissue preparation techniques, as per the respective protocol guidelines, do not account for the variability or sensitivity of starting material. Moreover, the shortcomings of the tested spin-column kits were likely related to the assumed standardized preparation of animal tissue rather than a reflection of the effectiveness of the column-based systems. The low A_{260}/A_{280} ratios and the inflated RNA yields observed with guanidinium thiocyanate solution (Trizol) indicated substandard extraction for high-throughput sequencing technology. This reagent was also discouraged due to the observed frequency of phenol contamination, which perturbs the RNA concentration and hinders downstream application³⁵. Thus, attenuating the risk of phenol contamination was of utmost importance given the high binding affinity of RNA to oxidized quinones in the presence of alcohol³⁶. Previous laryngeal muscle studies using this reagent to extract RNA from the rat model have only performed low-throughput analysis^{16–18,37–39}. In selecting an appropriate kit, this study valued a ~ 2.0 A_{260}/A_{280} ratio and a low variation between samples in consideration of the influence of batch effect during RNA-Seq analyses⁴⁰. The chosen kit provided the most favorable extracts with A_{260}/A_{280} ratios higher than 1.96, indicating successful DNase digestion. Consistent data void of chemical contamination across all assays also encouraged the use of this protocol. Though the standard method did not result in high RNA yields, it was the most practical complication to mitigate relative to other tested kits.

A limiting factor of the preferred kit was its inability to consistently provide sufficient total RNA without pooling muscle fibers ($pt = 3$). Compelling evidence in other rat model studies has demonstrated the feasibility of successful RNA-Seq analysis using the Aurum Total RNA Fatty and Fibrous Tissue Kit^{25,41}. Due to the greater column capacity (100 mg) of the aforementioned kit, its application can be assessed in future studies.

Assessment of recovered RNA revealed the significant influence of tissue preparation procedures, where RNA degradation remained inevitable upon organismal death until the development of the lysate. In downstream assessments, degradation, depicted by the loss of short genes and the changes to longer genes in the mRNA transcript, perturbs the innate gene profile⁴². Similar deficiencies can also persist during the large-scale amplification of extracts with low RNA quantities. Previous studies have also evinced organismal death and the *post-mortem* interval (PMI) as external factors that mediate alterations to tissue transcriptomes^{43–45}. Conversely, previous research has challenged the alterations to RNA integrity following prolonged ischemia finding no correlation between RNA quality and the PMI in human skeletal muscle and colonic epithelial tissue^{13,46}. Without a clear consensus in the literature, the present study mitigated degradation during the PMI by minimizing the total procedure time and employing RNase-inhibiting reagents⁴⁵. This study applied RNase-inhibiting reagent (RNAlater) to the dissected ILMs to limit degradation. Overnight incubation of the muscles in cold RNase-inhibiting reagent established the immobilization of active hydrolytic contributors during freeze/thaw cycles. ILM dissection from fresh tissue rather than after incubation in the stabilizing reagent allowed for efficient separation. Storing individual ILMs also increased the surface area exposed to the RNase-inhibiting reagent. Alternatively, incubating the whole larynx overnight would likely result in partial or fragmented muscle removal. Given the elevated RIN values and low 28S/18S ratios, this study concluded that the stability this reagent provided was not absolute. Previous methodological studies that assessed the efficiency of RNase-inhibiting reagents at different time points demonstrated reduced RIN after 24 h, justifying an overnight incubation^{34,47}.

Limitations using RNase-inhibiting reagents were related to their effectiveness over time. Namely, overnight storage in RNase-inhibiting reagents followed by prolonged storage at -80 °C was not assessed for changes in RNA integrity. Overnight storage was complicated by its propensity to cause column clogging and hole formation due to hardened ILMs that deemed several samples (23 out of 48) unusable (Table 1). Finally, due to the unreliability of the 28S/18S ratios, as shown in MTA muscles, this study could not draw any reliable conclusions apropos the efficiency of the reagent to enhance RNA stability. This study inferred RNA stability through visualization of the electropherogram peaks as such. Collectively, these results confirmed that this modification alone was insufficient for the consistent recovery of highly suitable RNA extracts.

The disruption paradigm developed here ameliorated structural and functional challenges associated with high-quality RNA isolation. Establishing an optimal method that leads to the destruction of the cell membrane without considerable deterioration of intracellular components was a rate-limiting step throughout this study. Heat generation resulting from intensive rotor–stator disruption cycles contributed to increased degradation in our samples—given the linear relationship between increasing temperature and RNA denaturation⁴⁸. The advantages of the developed method were four-fold. First, using an integrated homogenization strategy significantly increased the yield of RNA recovery per assay, allowing most extracts to qualify for RNA-Seq. Second, the ideal weight model permitted a systematic approach for optimal RNA extraction void of excessive inter- and intra-variability across the global experiments. Third, the conceptualization of the unique cryogenic disruption module provided an effective means for tissue disruption void of chemical and biological contaminants. Fourth, the experimental method reduced the incidence of column clogging and hole formation, making all recovered RNA applicable for bioanalyzer assessment (Table 1).

Limitations of the ideal weight model included observing no remarkable interaction between the span of rotor–stator disruption and the resultant RIN. Thus, because an accurate means to quantify the capacity of homogenization per ILM is unprecedented, the present method cannot guarantee extracts with RIN exclusively above 8.0. Alternatively, this protocol provides sufficient quantities of highly pure total RNA and RIN between 7.4 and 8.6 with limited variability compared to other skeletal muscles^{13,49}. The pronounced ILM sensitivity and the significant improvement of technical and biological challenges suggest the applicability of the experimental techniques to other skeletal muscles.

Although manual homogenization circumvented degradation from rotor–stator use, this technique alone provides insufficient RNA recovery for bulk RNA-Seq methods. Low RNA recovery can be problematic as it may lead to the overamplification of sequences not representative of the entire transcriptome^{50–52}. Manual homogenization is also more challenging to standardize due to the influence of human error. Maintaining consistent technical and biological conditions is essential for detecting outliers and variability of the sequencing data²⁷.

Given that increased variability may lead to unreliable RNA-Seq assessments, the present study recommends diligent manual lysis when a more sensitive library kit, such as TruSeq, is applied⁵³. Otherwise, the integrated method and a reasonable approach to determine the ideal load for cellular breakdown provide maximization of RNA with sufficient RIN values needed for high-throughput analysis (Table 1).

Given the restrictions of the spin columns (approximately 40 mg of starting material per column), pooling three ILMs per sample reflects both the minimum and the maximum amount needed for optimal RNA extraction of adult rat ILMs 100% of the time. Suitable RNA recovery is achievable using two ILMs, but only 88% of the time. A limitation of the proposed pooling strategy is the results may not accurately reflect population variation in gene expression levels⁵⁴. Pooling studies that evaluated differential gene expression previously reported high false positivity rates and pooling bias from pooling less than 8 tissues⁵⁴. Validation of RNA-Seq data using TruSeq, which notably allows for sequencing of degraded samples or low amounts of RNA, may be necessary to assess the impact of the experimental method⁵³.

The challenges regarding effective extraction for RNA-Seq analysis reflected the profound influence of degradation and structural differences between the ILMs. The present study observed differences in susceptibility to RNA degradation relative to the specific ILM (Supp. Fig. S2). One hypothesis to consider was that the ILM structure impacts optimal processing conditions. Recent findings demonstrating increased resistance of the rat PCA and TA muscles to functional impairment and age-related changes supported this hypothesis due to their physiological roles⁵⁵. This age-related study indicated that more resilient fibers in the PCA and TA muscles, relative to the cricoarytenoid muscle, are attributable to their inherent function. These observations suggested that the load required for the breakdown of the PCA is greater than that of the TA muscles due to their increased adaptive resistance and fiber content. Evaluating various purification strategies implicated degradation as particularly adverse for ILMs due to their small muscle fiber cross-sectional area and volume, ergo limited RNA abundance^{56,57}. Previous quantitative PCR analysis of abductor (PCA) and adductor (LTA and MTA) muscles also demonstrated the significant vulnerability of the cellular components of these muscles to damage during RNA isolation procedures¹³. In short, for optimal RNA extraction from rat ILMs, substantial force is needed to affect cell lysis; however, too much can compromise intact RNA (Supp. Fig. S2). Finally, our findings suggested the intrinsic characteristics of each muscle significantly impacted extraction. Thus, a systematic approach must be used to identify the force that will optimize RNA extraction for individual ILMs.

Conclusions

The present work demonstrates the hallmarks of critical factors that allowed for high-quality transcriptome analysis: stabilization of RNA provided by RNase-inhibiting agents, integrated homogenization, the ideal weight model, adapted cryogenic disruption, and tissue pooling. High-quality RNA extraction from the ILMs for general RNA-Seq analysis required additional consideration of the low amounts of starting material, handling of the specimen, tissue-specific composition, and tissue-specific degradation rates following death and excision. Comprehensive RNA-Seq analysis validated the efficacy of the experimental method identified herein, in general, and specifically for rat vocal ILM.

Methods

Animals. This study was performed in compliance with ARRIVE guidelines and the Public Health Service Policy on Humane Care and Use of Laboratory Animals, the National Institutes of Health Guide for the Care and Use of Laboratory Animals, and the Animal Welfare Act (7 U.S.C. et seq.). The Institutional Animal Care and Use Committee of Columbia University Medical Center approved the animal use protocol. Under a 12 h dark/light cycle and ambient temperature (21 °C), Sprague–Dawley rats were placed in group housing with ad libitum access to food and water. Young adult rats (~300 g) (n=482) were distributed in sets of triplicate treatment groups according to their sex (3 rats per group). The procedures and their modifications for the optimized protocol are described as follows:

Muscle tissue harvest. Adult rats were euthanized by a lethal injection of ketamine and xylazine before laryngeal muscle dissection. Once euthanized, 70% ethanol served as a skin disinfectant before harvesting the larynx. A midline incision was performed in the neck. Following retraction of submandibular glands and extralaryngeal muscles, the larynx was identified and removed en bloc with the proximal trachea, esophagus, and pharynx⁴⁰. The specimen was then transferred to a sterile petri dish and rinsed in 2 mL of RNAlater (catalogue #AM7021, Invitrogen, Vilnius, Lithuania), which served as a stabilizing agent. After aspirating excess solution from the petri dish, the specimen was placed onto a sterile surface for dissection via a Leica S8 APO compound microscope (Leica Microsystems, Buffalo Grove, IL). The esophagus and pharynx were carefully excised from the posterior aspect of the harvested tissue before extracting the right and left laryngeal abductor muscles (PCA). The aryepiglottic folds were then removed to provide access for dissection of the right and left adductor muscles (LTA and MTA) with fine-tip forceps. ILMs from the rat larynx were less than 5 mm in length, and individual muscle bellies weighed between 2 and 13 mg. Rather than storing the whole larynx in the reagent after rinsing, per other optimized protocols for RNA purification, individual ILMs were immediately incubated in 1 mL of RNAlater following dissection. Samples were then placed at 4°C overnight and then processed the following day.

Assessment of RNA extraction protocols. The following kits were tested for the evaluation of the most effective RNA isolation: ZR *Quick*-RNA MicroPrep (catalogue #R1051, Zymo Research, CA.), RNeasy Micro Kit (catalogue #74004, Qiagen, Hilden, Germany), TRIzol Reagent (catalogue #15596-026, Invitrogen Life Technologies, Carlsbad, CA, U.S.A.), and the Aurum Total RNA Mini Kit (catalogue #732-6820, Bio-Rad, Hercules,

CA, U.S.A.). In addition, the following procedures were evaluated: TRIzol protocol using a half volume of all reagents, Trizol in combination with RNeasy Mini kit (Qiagen), Trizol plus PureLink RNA Mini Kit (catalogue #12183018A, Invitrogen, Carlsbad, CA, U.S.A.), and RNAlater in sequential integration with the Aurum kit (Bio-Rad). RNA purification was followed according to the kit instructions, and deviations from the recommended preparation of the starting material are reported in the Results section. Protocol modifications to the Aurum kit and Trizol protocols facilitated the optimization of RNA purification. Here, parameters related to homogenization duration, disruption method, number of tissues per tube, and volume of reagents were modified.

Tissue preparation and processing. Before next-day isolation procedures, the benchtop was sprayed with RNaseZap (catalogue #AM9780, AM9782, Invitrogen, Waltham, MA, U.S.A.) for removing ribonuclease contamination. Other surfaces and instruments were also sprayed during all laboratory processes. The Aurum Total RNA Mini kit allowed for the most optimal and consistent extraction of high-quality RNA. For the prescribed procedure, tissues were removed from stabilizing reagent and briefly dabbed on a paper towel to remove excess solution, according to the manufacturer's guidelines. Samples were pooled ($pt=3$) according to muscle type, position (right or left), and gender. Similar laryngeal muscle tissues were combined in respective Bio-Masher III tubes (Nippi, Inc., Japan), with the filters removed, to facilitate manual grinding and lyophilization in liquid nitrogen via the disposable pestles. Before the physical breakdown of muscle tissue, the pooled samples were weighed to determine the appropriate duration of mechanical homogenization to yield cell lysates with significant intact RNA. After pooling, the calculated median total weights were 50 mg, 40 mg, and 20 mg for PCA, LTA, and MTA, respectively. An apparatus for cryogenic disruption was assembled using medium binder clips and BioMasherIII tubes (Fig. 4). After placing liquid nitrogen in the surgical tray, the pooled muscle fibers were broken down via a disposable pestle. For further muscle dissociation, the RNA-preserving denaturant (lysis buffer) was added to the lyophilized powder where samples were subject to additional disruption through repeated pipetting, following the Aurum kit protocol. The processing of outlier values with robust weights (PCA) was ameliorated by passing the lysate through two columns and aggregating the extracts in the last step. The breakdown of any remaining particulates via the pestle facilitated the blending of the lysate. Subsequently, mechanical homogenization ensued through rotor–stator disruption. Disposable probes were subject to cleansing in consecutive rounds of RNase-free water and 70% ethanol before automated lysing to avoid cross-contamination between samples. In all samples, disruption occurred in 1 min intervals to avoid heat generation derived from the TissueRuptor II (catalogue #9002755, Qiagen, MD)³⁴.

RNA extraction. RNA concentration was measured using a micro-volume spectrophotometer NanoDrop ONE (catalogue #ND-ONE-W, ThermoFisher, Wilmington, DE). RNA integrity, the value of which serves as the final determinant of efficacy for RNA-Seq analysis, was assessed using an Agilent 2100 bioanalyzer. The RNA integrity number (RIN) calculated using this software presents a range of values from 1.0 to 10.0—indicating complete degradation and intact RNA, respectively⁵⁸. This study aimed to reach RIN close to or higher than 8 for meaningful genomic analyses. The optimized protocol systematically yielded at least 500 ng total RNA, approximately 200 ng is generally required for RNA-seq.

Statistics. The present study expresses all data as mean \pm SD unless otherwise stated. All statistical analyses were performed using GraphPad Prism 9.3.1 (San Diego, CA). Ordinary one-way ANOVA followed by Dunnett's multiple comparisons tests were performed to compare the experimental results to the recovery of RNA using currently available protocols. A repeated analysis of variance followed by Tukey's post-hoc tests allowed for individual comparisons of the commercial extraction methods. To examine the effect of RNAlater and cryogenic disruption on RNA quality, two-way ANOVA followed by Bonferroni's multiple comparisons test was computed. The assessment of homogenization techniques and pooling strategies were facilitated by standard two-way ANOVA followed by Dunnett's multiple comparisons tests to assess RNA quantity and purity that resulted from cryogenic disruption. Linear regression analysis was performed to demonstrate the relationship of contributing factors in the ideal weight model. The data were tested for normality via Q-Q plot and regression analysis. Finally, data in all supplemental figures were computed by two-way ANOVA followed by Tukey's post-hoc tests. The present study considered $P < 0.05$ as the level of statistical significance. (* $P < 0.05$; ** $P < 0.01$; *** $P < 0.001$; **** $P < 0.0001$).

Data availability

The datasets generated and analyzed during the current study are available in the Gene Expression Omnibus (GEO) repository, <https://www.ncbi.nlm.nih.gov/geo/query/acc.cgi?acc=GSE217027>. Other data is available upon request from the corresponding author of this paper.

Received: 23 March 2022; Accepted: 2 December 2022

Published online: 15 December 2022

References

1. Famokunwa, B., Walsted, E. S. & Hull, J. H. Assessing laryngeal function and hypersensitivity. *Pulm. Pharmacol. Ther.* **56**, 108–115 (2019).
2. Vahabzadeh-Hagh, A. M., Pillutla, P., Zhang, Z. & Chhetri, D. K. Dynamics of intrinsic laryngeal muscle contraction. *Laryngoscope* **129**, E21–e25 (2019).
3. Choi, H. S., Berke, G. S., Ye, M. & Kreiman, J. Function of the posterior cricoarytenoid muscle in phonation: In vivo laryngeal model. *Otolaryngol. Head Neck Surg.* **109**, 1043–1051 (1993).

4. Hernández-Morato, I. *et al.* Reorganization of laryngeal motoneurons after crush injury in the recurrent laryngeal nerve of the rat. *J. Anat.* **222**, 451–461 (2013).
5. Hernández-Morato, I. *et al.* Somatotopic changes in the nucleus ambiguus after section and regeneration of the recurrent laryngeal nerve of the rat. *Anat. Rec.* **297**, 955–963 (2014).
6. Hernandez-Morato, I., Koss, S., Sharma, S. & Pitman, M. J. Influence of Netrin-1 on reinnervation of laryngeal muscles following recurrent laryngeal nerve injury. *Neurosci. Lett.* **653**, 244–249 (2017).
7. Pitman, M. J., Weissbrod, P., Roark, R., Sharma, S. & Schaefer, S. D. Electromyographic and histologic evolution of the recurrent laryngeal nerve from transection and anastomosis to mature reinnervation. *Laryngoscope* **121**, 325–331 (2011).
8. Tessema, B. *et al.* Evaluation of functional recovery of recurrent laryngeal nerve using transoral laryngeal bipolar electromyography: A rat model. *Ann. Otol. Rhinol. Laryngol.* **117**, 604–608 (2008).
9. Tessema, B. *et al.* Observations of recurrent laryngeal nerve injury and recovery using a rat model. *Laryngoscope* **119**, 1644–1651 (2009).
10. Sigurgeirsson, B., Emanuelsson, O. & Lundeberg, J. Sequencing degraded RNA addressed by 3' tag counting. *PLoS ONE* **9**, e91851 (2014).
11. Wang, Z., Gerstein, M. & Snyder, M. RNA-Seq: A revolutionary tool for transcriptomics. *Nat. Rev. Genet.* **10**, 57–63 (2009).
12. Stroh, A. M. *et al.* Human adipose and skeletal muscle tissue DNA, RNA, and protein content. *J. Appl. Physiol.* **131**, 1370–1379 (2021).
13. Koppelkamm, A., Vennemann, B., Lutz-Bonengel, S., Fracasso, T. & Vennemann, M. RNA integrity in post-mortem samples: Influencing parameters and implications on RT-qPCR assays. *Int. J. Legal Med.* **125**, 573–580 (2011).
14. Nouvel, A. *et al.* Optimization of RNA extraction methods from human metabolic tissue samples of the COMET biobank. *Sci. Rep.* **11**, 20975 (2021).
15. Bijangi-Vishehsaraei, K., Blum, K., Zhang, H., Safa, A. R. & Halum, S. L. Microarray analysis gene expression profiles in laryngeal muscle after recurrent laryngeal nerve injury. *Ann. Otol. Rhinol. Laryngol.* **125**, 247–256 (2015).
16. Hernandez-Morato, I., Isseroff, T. F., Sharma, S. & Pitman, M. J. Differential expression of glial-derived neurotrophic factor in rat laryngeal muscles during reinnervation. *Laryngoscope* **124**, 2750–2756 (2014).
17. Hernandez-Morato, I., Sharma, S. & Pitman, M. J. Changes in neurotrophic factors of adult rat laryngeal muscles during nerve regeneration. *Neuroscience* **333**, 44–53 (2016).
18. Horton, M. J., Rosen, C., Close, J. M. & Sciote, J. J. Quantification of myosin heavy chain RNA in human laryngeal muscles: Differential expression in the vertical and horizontal posterior cricoarytenoid and thyroarytenoid. *Laryngoscope* **118**, 472–477 (2008).
19. McMullen, C. A. & Andrade, F. H. Functional and morphological evidence of age-related denervation in rat laryngeal muscles. *J. Gerontol. Ser. A Biol. Sci. Med. Sci.* **64**, 435–442 (2009).
20. Montalbano, M. B. *et al.* Recurrent laryngeal nerve reinnervation in rats posttransection: Neurotrophic factor expression over time. *Otolaryngol. Head Neck Surg.* **161**, 111–117 (2019).
21. Padhi, B. K., Singh, M., Rosales, M., Pelletier, G. & Cakmak, S. A PCR-based quantitative assay for the evaluation of mRNA integrity in rat samples. *Biomolecular Detect. Quant.* **15**, 18–23 (2018).
22. Van Daele, D. J. Quantitative PCR analysis of laryngeal muscle fiber types. *J. Commun. Disord.* **43**, 327–334 (2010).
23. Cui, Q. *et al.* RNA sequencing (RNA-seq) analysis of gene expression provides new insights into hindlimb unloading-induced skeletal muscle atrophy. *Ann. Transl. Med.* **8**, 1595 (2020).
24. Shavlakadze, T. *et al.* Age-related gene expression signature in rats demonstrate early, late, and linear transcriptional changes from multiple tissues. *Cell Rep.* **28**, 3263–3273.e3263 (2019).
25. Lechner, S. A., Kletzien, H., Gammie, S. C. & Kelm-Nelson, C. A. Thyroarytenoid muscle gene expression in a rat model of early-onset Parkinson's disease. *Laryngoscope* **131**, E2874–E2879 (2021).
26. Palomares, M.-A. *et al.* Systematic analysis of TruSeq, SMARTer and SMARTer ultra-low RNA-seq kits for standard, low and ultra-low quantity samples. *Sci. Rep.* **9**, 7550 (2019).
27. Lungova, V., Chen, X., Wang, Z., Kendzioriski, C. & Thibeault, S. L. Human induced pluripotent stem cell-derived vocal fold mucosa mimics development and responses to smoke exposure. *Nat. Commun.* **10**, 4161 (2019).
28. Bailey, T. W. *et al.* RNA sequencing identifies transcriptional changes in the rabbit larynx in response to low humidity challenge. *BMC Genomics* **21**, 888 (2020).
29. Cannes do Nascimento, N., Dos Santos, A. P., Sivasankar, M. P. & Cox, A. Unraveling the molecular pathobiology of vocal fold systemic dehydration using an in vivo rabbit model. *PLoS ONE* **15**, e0236348–e0236348 (2020).
30. Lee, J.-H. *et al.* Molecular parallelism in fast-twitch muscle proteins in echolocating mammals. *Sci. Adv.* **4**, eaat9660 (2018).
31. Hoh, J. F. Y. Laryngeal muscle fibre types. *Acta Physiol. Scand.* **183**, 133–149 (2005).
32. Furtado, A. RNA extraction from developing or mature wheat seeds. In *Cereal Genomics: Methods and Protocols* (eds Henry, R. J. & Furtado, A.) 23–28 (Humana Press, 2014).
33. Moayed, Y. *et al.* The candidate splicing factor Sfswap regulates growth and patterning of inner ear sensory organs. *PLoS Genet.* **10**, e1004055 (2014).
34. Jun, E. *et al.* Method optimization for extracting high-quality RNA from the human pancreas tissue. *Transl. Oncol.* **11**, 800–807 (2018).
35. Unger, C., Lokmer, N., Lehmann, D. & Axmann, I. M. Detection of phenol contamination in RNA samples and its impact on qRT-PCR results. *Anal. Biochem.* **571**, 49–52 (2019).
36. Behnam, B. *et al.* An optimized isolation protocol yields high-quality RNA from cassava tissues (*Manihot esculenta* Crantz). *FEBS Open Bio* **9**, 814–825 (2019).
37. Araki, K. *et al.* Adenoviral GDNF gene transfer enhances neurofunctional recovery after recurrent laryngeal nerve injury. *Gene Ther.* **13**, 296–303 (2006).
38. Files, D. C. *et al.* The posterior cricoarytenoid muscle is spared from MuRF1-mediated muscle atrophy in mice with acute lung injury. *PLoS ONE* **9**, e87587 (2014).
39. Shiotani, A., O'Malley, B. W. Jr., Coleman, M. E. & Flint, P. W. Human insulinlike growth factor 1 gene transfer into paralyzed rat larynx: Single vs multiple injection. *Arch. Otolaryngol.-Head Neck Surg.* **125**, 555–560 (1999).
40. Koch, C. M. *et al.* A beginner's guide to analysis of RNA sequencing data. *Am. J. Respir. Cell Mol. Biol.* **59**, 145–157 (2018).
41. LoCoco, P. M. *et al.* Reliable approaches to extract high-integrity RNA from skin and other pertinent tissues used in pain research. *PAIN Rep.* **5**(2), e818 (2020).
42. Opitz, L. *et al.* Impact of RNA degradation on gene expression profiling. *BMC Med. Genomics* **3**, 36 (2010).
43. Bonadio, R. S. *et al.* Insights into how environment shapes post-mortem RNA transcription in mouse brain. *Sci. Rep.* **11**, 13008 (2021).
44. Ferreira, P. G. *et al.* The effects of death and post-mortem cold ischemia on human tissue transcriptomes. *Nat. Commun.* **9**, 490 (2018).
45. Sampaio-Silva, F., Magalhães, T., Carvalho, F., Dinis-Oliveira, R. J. & Silvestre, R. Profiling of RNA degradation for estimation of post mortem [corrected] interval. *PLoS ONE* **8**, e56507 (2013).
46. Galissier, T. *et al.* Biobanking of fresh-frozen human adenocarcinomatous and normal colon tissues: Which parameters influence RNA quality?. *PLoS ONE* **11**, e0154326–e0154326 (2016).
47. Heumüller-Klug, S. *et al.* Degradation of intestinal mRNA: A matter of treatment. *World J. Gastroenterol.* **21**, 3499–3508 (2015).

48. Mikulecky, P. J. & Feig, A. L. Heat capacity changes in RNA folding: Application of perturbation theory to hammerhead ribozyme cold denaturation. *Nucleic Acids Res.* **32**, 3967–3976 (2004).
49. Walker, D. G. *et al.* Characterization of RNA isolated from eighteen different human tissues: Results from a rapid human autopsy program. *Cell Tissue Banking* **17**, 361–375 (2016).
50. Bourgard, C., Lopes, S. C. P., Lacerda, M. V. G., Albrecht, L. & Costa, F. T. M. A suitable RNA preparation methodology for whole transcriptome shotgun sequencing harvested from *Plasmodium vivax*-infected patients. *Sci. Rep.* **11**, 5089 (2021).
51. Jaffe, A. E. *et al.* Profiling gene expression in the human dentate gyrus granule cell layer reveals insights into schizophrenia and its genetic risk. *Nat. Neurosci.* **23**, 510–519 (2020).
52. Parekh, S., Ziegenhain, C., Vieth, B., Enard, W. & Hellmann, I. The impact of amplification on differential expression analyses by RNA-seq. *Sci. Rep.* **6**, 25533 (2016).
53. Schuierer, S. *et al.* A comprehensive assessment of RNA-seq protocols for degraded and low-quantity samples. *BMC Genomics* **18**, 442 (2017).
54. Rajkumar, A. P. *et al.* Experimental validation of methods for differential gene expression analysis and sample pooling in RNA-seq. *BMC Genomics* **16**, 548 (2015).
55. Nishida, N. *et al.* Age-related changes in rat intrinsic laryngeal muscles: Analysis of muscle fibers, muscle fiber proteins, and subneural apparatuses. *Eur. Arch. Otorhinolaryngol.* **270**, 975–984 (2013).
56. Caiozzo, V. J., Wu, Y. Z., Baker, M. J. & Crumley, R. Effects of denervation on cell cycle control in laryngeal muscle. *Arch. Otolaryngol. Head Neck Surg.* **130**, 1056–1068 (2004).
57. Marguerat, S. & Bähler, J. Coordinating genome expression with cell size. *Trends Genet.* **28**, 560–565 (2012).
58. Schroeder, A. *et al.* The RIN: An RNA integrity number for assigning integrity values to RNA measurements. *BMC Mol. Biol.* **7**, 3 (2006).

Acknowledgements

We thank Almudena Bosch, Medini Annavajhala, and Larissa Williams for contributing their expertise in RNA-related studies; and the JP Sulzberger Columbia Genome Center for their services and assistance in next-generation sequencing. This work was supported by grant 1R01DC018060 of the US. National Institutes of Health to MJP.

Author contributions

Conceptualization: A.M.K., I.H.M., M.J.P. Methodology: A.M.K., I.H.M., Y.M., M.J.P. Formal analysis: A.M.K., I.H.M. Investigation: A.M.K. Resources: M.P. Data curation: A.M.K. writing—original draft: A.M.K. writing—review and editing: I.H.M., Y.M., M.J.P. Visualization: A.M.K., Supervision: M.J.P. Validation: A.M.K. Project administration: M.J.P. Funding acquisition: M.J.P.

Funding

This work was supported by the National Institutes of Health 1R01DC018060.

Competing interests

The authors declare no competing interests.

Additional information

Supplementary Information The online version contains supplementary material available at <https://doi.org/10.1038/s41598-022-25643-y>.

Correspondence and requests for materials should be addressed to I.H.-M.

Reprints and permissions information is available at www.nature.com/reprints.

Publisher's note Springer Nature remains neutral with regard to jurisdictional claims in published maps and institutional affiliations.



Open Access This article is licensed under a Creative Commons Attribution 4.0 International License, which permits use, sharing, adaptation, distribution and reproduction in any medium or format, as long as you give appropriate credit to the original author(s) and the source, provide a link to the Creative Commons licence, and indicate if changes were made. The images or other third party material in this article are included in the article's Creative Commons licence, unless indicated otherwise in a credit line to the material. If material is not included in the article's Creative Commons licence and your intended use is not permitted by statutory regulation or exceeds the permitted use, you will need to obtain permission directly from the copyright holder. To view a copy of this licence, visit <http://creativecommons.org/licenses/by/4.0/>.

© The Author(s) 2022